International Journal of Instrumentation Science 2013, 2(2): 13-24
DOI: 10.5923/j.instrument.20130202.01

Calculation of Full Energy Peak Efficiency of NaI (Tl) Detectors by New Analytical Approach for Cylindrical Sources

Ahmed M. El-Khatib, Mohamed S. Badawi, Mona M. Gouda*, Sherif S. Nafee, Ekram A. El-Mallah

Physics Department, Faculty of Science, Alexandria University, Alexandria, 21511, Egypt

Abstract A new analytical approach for calculation of the full-energy peak efficiency of NaI (Tl) is deduced. In addition, self attenuation of the source matrix, the attenuation by the source container and the detector housing materials are considered in the mathematical treatment. Results are compared with those measured by two cylindrical NaI (Tl) detectors with Resolution (FWHM) at 662 keV equal to 7.5% and 8.5%. ^{152}Eu aqueous radioactive sources covering the energy range from 121 keV to 1408 keV were used. By comparison, the calculated and the measured full-energy peak efficiency values were in a good agreement.

Keywords Nai (Tl) Scintillation Detectors, Cylindrical Sources, Full-Energy Peak Efficiency, Self-Attenuation

1. Introduction

NaI (Tl) detectors are commonly used to identify and measure activities of low-level radioactive sources. They have high detection efficiency and operate at room temperature[1]. The determination of the activity for each radionuclide requires prior knowledge of the full-energy peak efficiency at each photon energy for a given measuring geometry, which must be obtained by an efficiency calibration using known standard sources of exactly the same geometrical dimensions, density, and chemical composition of the sample under study. Standard radioactive samples, if available, are costly and would need to be renewed, especially when the radionuclides have short half-lives[2]. In addition, the influence of the source matrix on the counting efficiency can be expressed by the self-attenuation factor, describing the fraction of gamma-rays not registered in the full-energy peak due to scattering or absorption within the sample[3]. An effective tool to overcome these problems could be the use of computational techniques[4-9] to complete calibration of the gamma spectrometry system. Also, Selim and Abbas [10-14] solved this problem by derived direct analytical integrals of the detector efficiencies (total and full-energy peak) for any source-detector configuration and implemented these analytical expressions into a numerical integration computer program. Moreover, they introduced a new theoretical approach[15-17] based on that Direct Statistical method to determine the detector efficiency for an isotropic radiating point source at any arbitrary position from a cylindrical detector, as well as the extension of this approach to evaluate the volumetric sources.

In the present work, authors will modify this simplified approach to determine the full-energy peak efficiency of the co-axial detector with respect to point and volumetric sources, taking into account the attenuation by the dead layer (reflector) and the end-cap material of the detector, the self attenuation by the source matrix and finally, the attenuation by the source container material.

* Corresponding author:
ahec3@yahoo.com (Mona M. Gouda)
Published online at http://journal.sapub.org/instrument

2. Mathematical Viewpoint

2.1. The Case of a Non-axial Point Source

Consider a right circular cylindrical (2R × L), detector and an arbitrarily positioned isotropic radiating point source located at a distance h from the detector top surface, and at a lateral distance ρ from its axis. The efficiency of the detector with respect to point source is given as follows[16]:

$$\varepsilon_{point} = f_{att}\,\varepsilon_g\,\varepsilon_i \qquad (1)$$

Where ε_i and ε_g are the intrinsic and the geometrical efficiencies which are derived by Abbas et al., [16]. f_{att} is the attenuation factor of the detector dead layer and end cap material. In section 2.1.2, this factor will be recalculated by a new method which is dependent on calculating the average path length within these materials.

2.1.1. The Intrinsic (ε_i) and the Geometrical (ε_g) Efficiencies

The intrinsic and geometrical efficiencies are represented by Eqs. (2) and (3) respectively.

$$\varepsilon_i = 1 - e^{-\mu \bar{d}} \tag{2}$$

$$\varepsilon_g = \frac{\Omega}{4\pi} \tag{3}$$

Where $\bar{d}$ is the average path length travelled by a photon through the detector, Ω is the solid angle subtended by the source-detector and they are represented by Eqs. (4) and (5) respectively. μ is the attenuation coefficient of the detector material.

$$\bar{d} = \frac{\int_{\Omega} d(\theta,\varphi)\, d\Omega}{\int_{\Omega} d\Omega} = \frac{\int_{\varphi}\int_{\theta} d(\theta,\varphi)\sin\theta\, d\theta\, d\varphi}{\Omega} \tag{4}$$

Where θ and φ are the polar and the azimuthal angles respectively. $d(\theta,\varphi)$ is the possible path length travelled by the photon within the detector active volume.

$$\Omega = \int_{\varphi}\int_{\theta} \sin\theta\, d\theta\, d\varphi \tag{5}$$

There are two main cases to be considered for calculating the intrinsic and geometrical efficiencies of the detector with respect to point source, viz., (i) the lateral displacement of the source is smaller than or equa0l the detector circular face's radius ($\rho \leq R$) and (ii) the lateral distance of the source is greater than the detector circular face's radius ($\rho > R$). The two cases have been treated by Abbas et al.,[16]. The values of the polar and the azimuthal angles based on the source to detector configuration are shown in Table 1.

Table 1. The Values of the Polar and the Azimuthal Angles Based on the Source to Detector Configuration

The polar angles	The azimuthal angles
$\theta_1 = \tan^{-1}\left(\frac{\lvert R-\rho\rvert}{h+L}\right)$	
$\theta_2 = \tan^{-1}\left(\frac{\lvert R-\rho\rvert}{h}\right)$	
$\theta_3 = \tan^{-1}\left(\frac{R+\rho}{h+L}\right)$	$\varphi_{\max} = \cos^{-1}\left(\frac{\rho^2 - R^2 + h^2\tan^2\theta}{2\rho h\tan\theta}\right)$
$\theta_4 = \tan^{-1}\left(\frac{R+\rho}{h}\right)$	$\varphi'_{\max} = \cos^{-1}\left(\frac{\rho^2 - R^2 + (h+L)^2\tan^2\theta}{2\rho(h+L)\tan\theta}\right)$
$\theta_c = \tan^{-1}\left(\frac{\sqrt{\rho^2 - R^2}}{h+L}\right)$	$\varphi_c = \sin^{-1}\left(\frac{R}{\rho}\right)$
$\theta_c' = \tan^{-1}\left(\frac{\sqrt{\rho^2 - R^2}}{h}\right)$	
$\theta_T = \tan^{-1}\left(\frac{\sqrt{\rho^2 - R^2}}{\sqrt{h(h+L)}}\right)$ $(\varphi_{\max} = \varphi'_{\max})$	

2.1.2. The Attenuation Factor (f_{att})

The attenuation factor f_{att} is expressed as:

$$f_{att} = f_{lay}\ f_{cap} \tag{6}$$

where f_{lay} and f_{cap} are the attenuation factors of the detector dead layer and end cap material respectively and they are given by:

$$f_{lay} = e^{-\mu_{lay}\,\overline{\delta_{lay}}},\ f_{cap} = e^{-\mu_{cap}\,\overline{\delta_{cap}}} \tag{7}$$

where μ_{lay} and μ_{cap} are the attenuation coefficients of the detector dead layer and the end cap material, respectively. While $\overline{\delta_{lay}}$ and $\overline{\delta_{cap}}$ are the average path length travelled by a photon through the detector dead layer and end cap material, respectively. They are represented as follow:

$$\left.\begin{aligned}\overline{\delta_{lay}} &= \frac{\int_{\varphi}\int_{\theta} t'(\theta,\varphi)\sin\theta\, d\theta\, d\varphi}{\int_{\varphi}\int_{\theta}\sin\theta\, d\theta\, d\varphi} = \frac{\int_{\varphi}\int_{\theta} t'(\theta,\varphi)\sin\theta\, d\theta\, d\varphi}{\Omega} \\ \overline{\delta_{cap}} &= \frac{\int_{\varphi}\int_{\theta} t''(\theta,\varphi)\sin\theta\, d\theta\, d\varphi}{\int_{\varphi}\int_{\theta}\sin\theta\, d\theta\, d\varphi} = \frac{\int_{\varphi}\int_{\theta} t''(\theta,\varphi)\sin\theta\, d\theta\, d\varphi}{\Omega}\end{aligned}\right\} \quad (8)$$

Table 2. The Possible Path Lengths and the Average Path Length Traveled by the Photon Within the Dead Layer for Cases $\rho \le R$ and $\rho > R$

$\rho \le R$	$\rho > R$
$t_1' = \frac{t_{DF}}{\cos\theta}$	$t_1' = \frac{t_{DF}}{\cos\theta}$ $t_2' = \frac{\rho\cos\varphi + \sqrt{\left(R + t_{DS}\right)^2 - \rho^2\sin^2\varphi}}{\sin\theta} - \frac{\rho\cos\varphi + \sqrt{\left(R\right)^2 - \rho^2\sin^2\varphi}}{\sin\theta} \cong \frac{t_{DS}\left(1 + \frac{\rho^2}{2R^2}\sin^2\varphi\right)}{\sin\theta}$
$\overline{\delta_{lay}} = \frac{Z_1}{I_2}$	$\overline{\delta_{lay}} = \frac{Z_3}{I_4}$
$Z_1 = \int_0^{\pi}\int_0^{\theta_2} t_1' \sin\theta\, d\theta\, d\varphi + \int_0^{\varphi_{\max}}\int_{\theta_2}^{\theta_4} t_1' \sin\theta\, d\theta\, d\varphi$	$Z_3 = \int_{\theta_1}^{\theta_2}\int_0^{\varphi'_{\max}} t_2' \sin\theta\, d\varphi\, d\theta + \int_{\theta_2}^{\theta'_c}\int_0^{\varphi'_{\max}} t_1' \sin\theta\, d\varphi\, d\theta + \int_{\theta'_c}^{\theta_c}\int_0^{\varphi_c} t_1' \sin\theta\, d\varphi\, d\theta + \int_{\theta_c}^{\theta_4}\int_0^{\varphi_{\max}} t_1' \sin\theta\, d\varphi\, d\theta$ ($\theta_2 \ge \theta'_c$) $Z_3 = \int_{\theta_1}^{\theta'_c}\int_0^{\varphi'_{\max}} t_2' \sin\theta\, d\varphi\, d\theta + \int_{\theta'_c}^{\theta_2}\int_0^{\varphi_c} t_2' \sin\theta\, d\varphi\, d\theta + \int_{\theta_2}^{\theta_c}\int_0^{\varphi_c} t_1' \sin\theta\, d\varphi\, d\theta + \int_{\theta_c}^{\theta_4}\int_0^{\varphi_{\max}} t_1' \sin\theta\, d\varphi\, d\theta$ ($\theta_2 < \theta'_c$)

Where $t'(\theta,\varphi)$ and $t''(\theta,\varphi)$ are the possible path lengths travelled by the photon within the detector dead layer and end cap material, respectively.

Consider the detector has a dead layer by covering its upper surface with thickness t_{DF} and its side surface with thickness t_{DS}, (see Figure 1). The possible path lengths and the average path length travelled by the photon within the dead layer for cases ($\rho \le R$) and ($\rho > R$) are shown in Table 2, where t_1' and t_2' represents the photon path length through the upper and the side surface of the dead layer respectively.

Consider the thickness of upper and side surface of the detector end cap material is t_a and t_w respectively, as shown in Figure 1. The possible path lengths and the average path length travelled by the photon within the detector end cap material for cases ($\rho \le R$) and ($\rho > R$) are shown in Table 3, where t_1'' and t_2'' represents the photon path length through the upper and the side surface of the detector end cap material, respectively. From Table 4 we observe that, the case in which ($\rho > R$) has two sub cases which are ($R < \rho \le R_a$) and ($\rho > R_a$), where R_a is the inner radius of the detector end cap. There is a very important polar angle (θ_{cap}) which must be considered when we study the case in which ($\rho > R_a$) which is θ_{cap} and this is given by:

$$\theta_{cap} = \tan^{-1}\left(\frac{\rho - R_a}{h - k}\right) \quad (9)$$

Where k is the distance between the detector end cap and the detector upper surface.

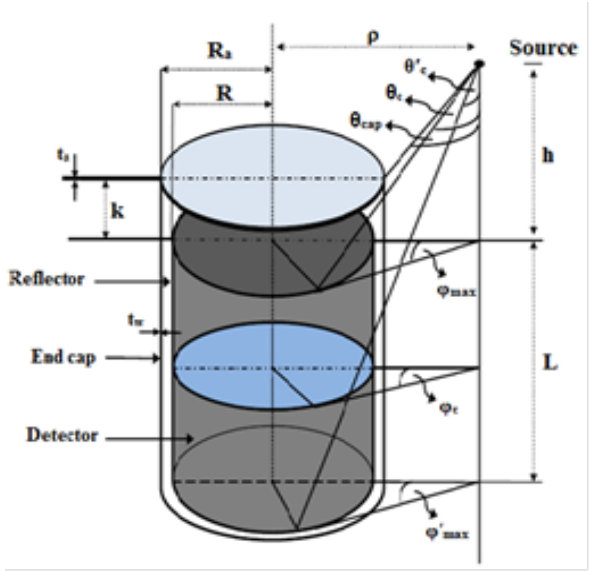

Figure 1. A diagram of a cylindrical –type detector with a non-axial point source (ρ>R)

2.2. The Case of a Co-axial Cylindrical Source

The efficiency of a cylindrical detector with radius R and height L using a cylindrical source with radius S and height H is given by:

$$\varepsilon_{cyl} = \frac{S_{self}\, S_{sc}\, f_{att}\, \varepsilon_i\, \varepsilon_g}{V} \tag{10}$$

where V is the volume of the cylindrical source ($V = \pi S^2 H$), S_{self} is the self attenuation factor of the source matrix and S_{sc} is the attenuation factor of the source container material.

If the source is over the surface of the detector, one has to consider two main cases. The first one is the case where the radius of the source is smaller than or equal to the detector circular face's radius (S≤R) and the second one is the case where the radius of the source is greater than to the detector circular face's radius (S>R), so that, one will discuss Eq. (10) for each case separately as follow:

2.2.1. Cylindrical Source with Radius Smaller than or Equal to the Detector's Radius (S≤R)

The intrinsic and geometrical efficiencies are as identified before in Eqs. (2) and (3) respectively, but the average path length $\overline{d}$ traveled by the photon through the detector active volume and the solid angle will have new forms due to the geometry of the volumetric source, as shown in Figure 2. The average path length is expressed as:

$$\overline{d} = \frac{\int_{h_o}^{H+h_o}\int_{0}^{2\pi}\int_{0}^{S} I_1(\rho \le R)\,\rho\, d\rho\, d\alpha\, dh}{\int_{h_o}^{H+h_o}\int_{0}^{2\pi}\int_{0}^{S} I_2(\rho \le R)\,\rho\, d\rho\, d\alpha\, dh} \tag{11}$$

Where I_1 and I_2 are the numerator and the denominator of $\overline{d}$ equation obtained by Abbas et al.(2006) for non axial point source (ρ≤R). α is the angle between the lateral distance ρ and the detector's major axis. The geometrical efficiency ε_g is given by:

$$\varepsilon_g = \frac{\int_{h_o}^{H+h_o}\int_{0}^{2\pi}\int_{0}^{S} I_2(\rho \le R)\,\rho\, d\rho\, d\alpha\, dh}{2\pi} \tag{12}$$

The new forms of the average path length travelled by the photon through the detector dead layer and the detector end cap material are given by Eqs. (13) and (14) respectively.

$$\overline{\delta_{lay}} = \frac{\int_{h_o}^{H+h_o}\int_{0}^{2\pi}\int_{0}^{S} Z_1\,\rho\, d\rho\, d\alpha\, dh}{\int_{h_o}^{H+h_o}\int_{0}^{2\pi}\int_{0}^{S} I_2(\rho \le R)\,\rho\, d\rho\, d\alpha\, dh} \tag{13}$$

where Z_1 is as identified before in Table 2.

where Z_1' is as identified before in Table 3.

In the case of a co-axial cylindrical source with radius S smaller than the detector radius R, there are two photon possible path lengths to leave the source as follow:

i . To exit from the base

$$t_1 = \frac{h - h_o}{\cos\theta} \tag{15}$$

ii . To exit from the side

$$t_2 = \frac{\rho\cos\varphi + \sqrt{S^2 - \rho^2\sin^2\varphi}}{\sin\theta} \tag{16}$$

Where h_o is the distance between the source active volume and the detector upper surface. The polar and the azimuthal angles will take the values:

$$\begin{aligned}
\theta_1' &= \tan^{-1}\left(\frac{S-\rho}{h-h_o}\right)\\
\theta_3' &= \tan^{-1}\left(\frac{S+\rho}{h-h_o}\right)\\
\varphi_s &= \cos^{-1}\left(\frac{\rho^2 - S^2 + (h-h_o)^2\tan^2\theta}{2(h-h_o)\rho\tan\theta}\right)\\
\theta_T &= \tan^{-1}\sqrt{\frac{(R^2-S^2)}{h_o(h-h_o)} - \frac{(R^2-\rho^2)}{h(h-h_o)}} \qquad (\varphi_S = \varphi_{\max}\ at\ \theta = \theta_T)
\end{aligned} \tag{17}$$

Where φ_s is the maximum azimuthal angle for the photon to emerge from the bottom of the source.

$$\overline{\delta_{cap}} = \frac{\int_{h_o}^{H+h_o}\int_{0}^{2\pi}\int_{0}^{S} Z_1'\,\rho\, d\rho\, d\alpha\, dh}{\int_{h_o}^{H+h_o}\int_{0}^{2\pi}\int_{0}^{S} I_2(\rho \le R)\,\rho\, d\rho\, d\alpha\, dh} \tag{14}$$

Table 3. The Possible Path Lengths and the Average Path Length Traveled by the Photon Within the Detector End Cap Material for Cases $\rho \leq R$ and $\rho > R$

$\rho \leq R$	$\rho > R$	
	$R < \rho \leq R_a$	$\rho > R_a$
$t_1'' = \dfrac{t_a}{\cos\theta}$	$t_1'' = \dfrac{t_a}{\cos\theta}$	$t_1'' = \dfrac{t_a}{\cos\theta}$ $t_2'' = \dfrac{\rho\cos\varphi + \sqrt{(R_a + t_w)^2 - \rho^2\sin^2\varphi}}{\sin\theta}$ $- \dfrac{\rho\cos\varphi + \sqrt{(R_a)^2 - \rho^2\sin^2\varphi}}{\sin\theta} \cong \dfrac{t_w\left(1 + \dfrac{\rho^2}{2R_a{}^2}\sin^2\varphi\right)}{\sin\theta}$
$\overline{\delta_{cap}} = \dfrac{Z_1'}{I_2}$	$\overline{\delta_{cap}} = \dfrac{Z_3'}{I_4}$	$\overline{\delta_{cap}} = \dfrac{Z_3'}{I_4}$
$Z_1' = \int_0^{\pi}\int_0^{\theta_2} t_1''\sin\theta\, d\theta\, d\varphi + \int_0^{\varphi_{\max}}\int_{\theta_2}^{\theta_4} t_1''\sin\theta\, d\theta\, d\varphi$	$Z_3' = \int_{\theta_1}^{\theta_c'}\int_0^{\varphi_{\max}'} t_1''\sin\theta\, d\varphi\, d\theta + \int_{\theta_c'}^{\theta_c}\int_0^{\varphi_c} t_1''\sin\theta\, d\varphi\, d\theta + \int_{\theta_c}^{\theta_4}\int_0^{\varphi_{\max}} t_1''\sin\theta\, d\varphi\, d\theta$	$Z_3' = \int_{\theta_1}^{\theta_c'}\int_0^{\varphi_{\max}'} t_1''\sin\theta\, d\varphi\, d\theta + \int_{\theta_c'}^{\theta_c}\int_0^{\varphi_c} t_1''\sin\theta\, d\varphi\, d\theta + \int_{\theta_c}^{\theta_4}\int_0^{\varphi_{\max}} t_1''\sin\theta\, d\varphi\, d\theta$ ($\theta_1 \geq \theta_{cap}$) $Z_3' = \int_{\theta_1}^{\theta_{cap}}\int_0^{\varphi_{\max}'} t_2''\sin\theta\, d\varphi\, d\theta + \int_{\theta_{cap}}^{\theta_c'}\int_0^{\varphi_{\max}'} t_1''\sin\theta\, d\varphi\, d\theta + \int_{\theta_c'}^{\theta_c}\int_0^{\varphi_c} t_1''\sin\theta\, d\varphi\, d\theta + \int_{\theta_c}^{\theta_4}\int_0^{\varphi_{\max}} t_1''\sin\theta\, d\varphi\, d\theta$ ($\theta_c' > \theta_{cap}$)

$Z_3' = \int_{\theta_1}^{\theta_c'} \int_{0}^{\varphi_{\max}'} t_2'' \sin\theta \, d\varphi \, d\theta + \int_{\theta_c'}^{\theta_{cap}} \int_{0}^{\varphi_c} t_2'' \sin\theta \, d\varphi \, d\theta + \int_{\theta_{cap}}^{\theta_c} \int_{0}^{\varphi_c} t_1'' \sin\theta \, d\varphi \, d\theta + \int_{\theta_c}^{\theta_4} \int_{0}^{\varphi_{\max}} t_1'' \sin\theta \, d\varphi \, d\theta$		$\theta_{cap} \geq \theta'_c$
$Z_3' = \int_{\theta_1}^{\theta_c'} \int_{0}^{\varphi_{\max}'} t_2'' \sin\theta \, d\varphi \, d\theta + \int_{\theta_c'}^{\theta_c} \int_{0}^{\varphi_c} t_2'' \sin\theta \, d\varphi \, d\theta + \int_{\theta_c}^{\theta_{cap}} \int_{0}^{\varphi_{\max}} t_2'' \sin\theta \, d\varphi \, d\theta + \int_{\theta_{cap}}^{\theta_4} \int_{0}^{\varphi_{\max}} t_1'' \sin\theta \, d\varphi \, d\theta$		$\theta_4 > \theta_{cap} \geq \theta_c$
$Z_3' = \int_{\theta_1}^{\theta_c'} \int_{0}^{\varphi_{\max}'} t_2'' \sin\theta \, d\varphi \, d\theta + \int_{\theta_c'}^{\theta_c} \int_{0}^{\varphi_c} t_2'' \sin\theta \, d\varphi \, d\theta + \int_{\theta_c}^{\theta_4} \int_{0}^{\varphi_{\max}} t_2'' \sin\theta \, d\varphi \, d\theta$		$\theta_{cap} \geq \theta_4$

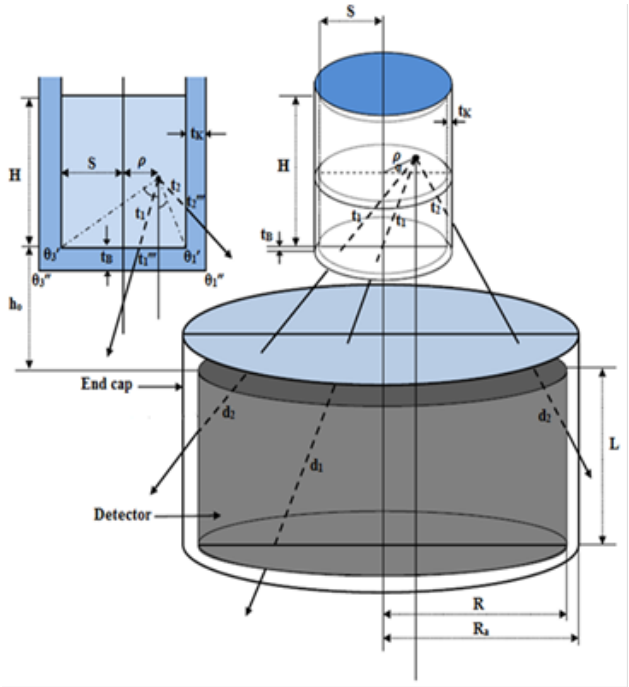

Figure 2. The possible cases of the photon path lengths through source – detector system (S≤R)

The self attenuation factor of the source matrix is given by:

$$S_{self} = e^{-\mu_s \bar{t}} \tag{18}$$

Where μ_s is the attenuation coefficient of the source matrix and $\bar{t}$ is the average path length travelled by a photon inside the source and is given by:

$$\bar{t} = \frac{\int_{h_o}^{H+h_o}\int_0^{\pi}\int_0^{S} g_1 \rho\, d\rho\, d\alpha\, dh}{\int_{h_o}^{H+h_o}\int_0^{\pi}\int_0^{S} I_2(\rho \le R)\rho\, d\rho\, d\alpha\, dh} \tag{19}$$

with

$$g_1 = \int_{\varphi}\int_{\theta} t(\theta,\varphi)\sin\theta\, d\theta\, d\varphi \tag{20}$$

There are three cases for the values of g_1 according to the values of the polar angle θ_i as follow:

i. The case in which ($\theta_4 > \theta_3'$ and $\theta_2 > \theta_1'$)

$$\begin{aligned} g_1 = {} & \pi\int_0^{\theta_1'} t_1 \sin\theta\, d\theta + \int_{\theta_1'}^{\theta_3}\varphi_s t_1 \sin\theta\, d\theta + \int_{\theta_1'}^{\theta_2}\int_0^{\pi} t_2 \sin\theta\, d\varphi\, d\theta \\ & - \int_{\theta_1'}^{\theta_3}\int_0^{\varphi_s} t_2 \sin\theta\, d\varphi\, d\theta + \int_{\theta_2}^{\theta_4}\int_0^{\varphi_{\max}} t_2 \sin\theta\, d\varphi\, d\theta \end{aligned} \tag{21}$$

ii. The case in which ($\theta_3' \ge \theta_4$ and $\theta_1' \ge \theta_2$)

$$g_1 = \pi\int_0^{\theta_2} t_1 \sin\theta\, d\theta + \int_{\theta_2}^{\theta_4}\varphi_{\max} t_1 \sin\theta\, d\theta \tag{22}$$

iii. The case in which ($\theta_3' \ge \theta_4$ and $\theta_1' < \theta_2$)

$$\begin{aligned} g_1 = {} & \pi\int_0^{\theta_1'} t_1 \sin\theta\, d\theta + \int_{\theta_1'}^{\theta_T}\varphi_s t_1 \sin\theta\, d\theta + \int_{\theta_T}^{\theta_4}\varphi_{\max} t_1 \sin\theta\, d\theta \\ & + \int_{\theta_1'}^{\theta_2}\int_0^{\pi} t_2 \sin\theta\, d\varphi\, d\theta - \int_{\theta_1'}^{\theta_T}\int_0^{\varphi_s} t_2 \sin\theta\, d\varphi\, d\theta + \int_{\theta_2}^{\theta_T}\int_0^{\varphi_{\max}} t_2 \sin\theta\, d\varphi\, d\theta \end{aligned} \tag{23}$$

If t_B is the source container bottom thickness and t_K is the source container side thickness, so, there are two photon possible path lengths to exit from the source container as follow:

i. Ⅰ. To exit from the base

$$t_1''' = \frac{t_B}{\cos\theta} \tag{24}$$

ii. Ⅱ. To exit from the side

$$t_2''' = \frac{\rho\cos\varphi + \sqrt{(S+t_K)^2 - \rho^2\sin^2\varphi}}{\sin\theta} - \frac{\rho\cos\varphi + \sqrt{(S)^2 - \rho^2\sin^2\varphi}}{\sin\theta} \cong \frac{t_K\left(1+\frac{\rho^2}{2S^2}\sin^2\varphi\right)}{\sin\theta} \tag{25}$$

The polar and the azimuthal angles can take the values:

$$\left.\begin{aligned} \theta_1'' &= \tan^{-1}\left(\frac{S+t_K-\rho}{h-h_0}\right) \\ \theta_3'' &= \tan^{-1}\left(\frac{S+t_K+\rho}{h-h_0}\right) \\ \varphi_s' &= \cos^{-1}\left(\frac{\rho^2-(S+t_K)^2+(h-h_o)^2\tan^2\theta}{2(h-h_o)\rho\tan\theta}\right) \\ \theta_T' &= \tan^{-1}\sqrt{\frac{(R^2-(S+t_K)^2)}{h_o(h-h_o)}-\frac{(R^2-\rho^2)}{h(h-h_o)}} \qquad (\varphi_S' = \varphi_{\max}\ at\ \theta=\theta_T') \end{aligned}\right\} \tag{26}$$

Where φ_s' is the maximum azimuthal angle for the photon to emerge from the bottom of the source container. The attenuation factor of the container material is given by:

$$S_{SC} = e^{-\mu_C \overline{t_c}} \tag{27}$$

Where μ_c is the attenuation coefficient of the source container material and $\overline{t_c}$ is the average path length travelled by a photon inside the source container and is expressed as:

$$\bar{t}_C = \frac{\int_{h_o}^{H+h_o}\int_0^{\pi}\int_0^{S} g_{1c}\,\rho\,d\rho\,d\alpha\,dh}{\int_{h_o}^{H+h_o}\int_0^{\pi}\int_0^{S} I_2(\rho\le R)\,\rho\,d\rho\,d\alpha\,dh} \tag{28}$$

with

$$g_{1c} = \int_{\varphi}\int_{\theta} t'''(\theta,\varphi)\sin\theta\,d\theta\,d\varphi \tag{29}$$

There are three cases for the values of g_{1c} according to the values of the polar angles θ_i as follow:

i . The case in which ($\theta_4 > \theta_3''$ and $\theta_2 > \theta_1''$)

$$\begin{aligned} g_{1c} = {} & \pi\int_0^{\theta_1''} t_1'''\sin\theta\,d\theta + \int_{\theta_1''}^{\theta_3''}\varphi_s' t_1'''\sin\theta\,d\theta + \int_{\theta_1''}^{\theta_2}\int_0^{\pi} t_2'''\sin\theta\,d\varphi\,d\theta \\ & - \int_{\theta_1''}^{\theta_3''}\int_0^{\varphi_s'} t_2'''\sin\theta\,d\varphi\,d\theta + \int_{\theta_2}^{\theta_4}\int_0^{\varphi_{\max}} t_2'''\sin\theta\,d\varphi\,d\theta \end{aligned} \tag{30}$$

ii . The case in which ($\theta_3'' \ge \theta_4$ and $\theta_1'' \ge \theta_2$)

$$g_{1c} = \pi\int_0^{\theta_2} t_1'''\sin\theta\,d\theta + \int_{\theta_2}^{\theta_4}\varphi_{\max} t_1'''\sin\theta\,d\theta \tag{31}$$

iii. The case in which ($\theta_3'' \ge \theta_4$ and $\theta_1'' < \theta_2$)

$$\begin{aligned} g_{1c} = {} & \pi\int_0^{\theta_1''} t_1'''\sin\theta\,d\theta + \int_{\theta_1''}^{\theta_T'}\varphi_s' t_1'''\sin\theta\,d\theta + \int_{\theta_T'}^{\theta_4}\varphi_{\max} t_1'''\sin\theta\,d\theta \\ & + \int_{\theta_1''}^{\theta_2}\int_0^{\pi} t_2'''\sin\theta\,d\varphi\,d\theta - \int_{\theta_1''}^{\theta_T'}\int_0^{\varphi_s'} t_2'''\sin\theta\,d\varphi\,d\theta + \int_{\theta_2}^{\theta_T'}\int_0^{\varphi_{\max}} t_2'''\sin\theta\,d\varphi\,d\theta \end{aligned} \tag{32}$$

2.2.2. Cylindrical Source with Radius Greater than the Detector's Radius (S>R)

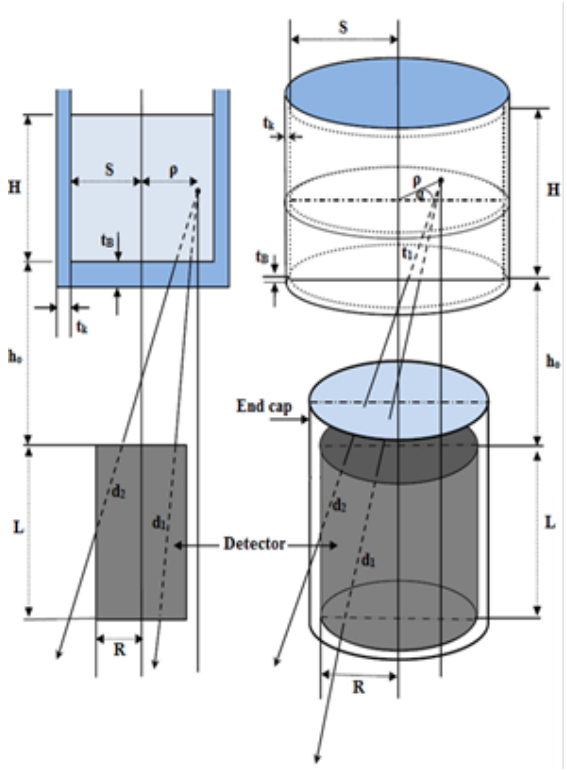

Figure 3. The possible cases of the photon path lengths through source – detector system (S>R)

The average path length $\overline{d}$ travelled by the photon through the detector active volume and the solid angle will take new forms due to the geometry of the volumetric source, as shown in Figure 3. The average path length is expressed as:

$$\overline{d}=\frac{\int_{h_o}^{H+h_o}\int_{0}^{2\pi}(\int_{0}^{R}I_1(\rho\le R)\rho d\rho+\int_{R}^{S}I_1(\rho>R)\rho\, d\rho)d\alpha\, dh}{\int_{h_o}^{H+h_o}\int_{0}^{2\pi}(\int_{0}^{R}I_2(\rho\le R)\rho d\rho+\int_{R}^{S}I_2(\rho>R)\rho d\rho)d\alpha\, dh} \quad (33)$$

Where I_1 and I_2 are the numerator and the denominator of $\overline{d}$ equation obtained by Abbas et al.(2006) for non axial point source. α is the angle between the lateral distance ρ and the detector's major axis. The geometrical efficiency ε_g is given by:

$$\varepsilon_g=\frac{\int_{h_o}^{H+h_o}\int_{0}^{2\pi}(\int_{0}^{R}I_2(\rho\le R)\rho d\rho+\int_{R}^{S}I_2(\rho>R)\rho d\rho)d\alpha\, dh}{2\pi} \quad (34)$$

The new forms of the average path length travelled by the photon through the detector dead layer and the detector end cap material are given by Eqs. (35) and (36) respectively.

$$\overline{\delta_{lay}}=\frac{\int_{h_o}^{H+h_o}\int_{0}^{2\pi}(\int_{0}^{R}Z_1\rho d\rho+\int_{R}^{S}Z_3\rho d\rho)d\alpha\, dh}{\int_{h_o}^{H+h_o}\int_{0}^{2\pi}(\int_{0}^{R}I_2(\rho\le R)\rho d\rho+\int_{R}^{S}I_2(\rho>R)\rho d\rho)d\alpha\, dh} \quad 35)$$

where Z_1 and Z_3 are as identified before in Table 2.

$$\overline{\delta_{cap}}=\frac{\int_{h_o}^{H+h_o}\int_{0}^{2\pi}(\int_{0}^{R}Z_1'\rho d\rho+\int_{R}^{S}Z_3'\rho d\rho)d\alpha\, dh}{\int_{h_o}^{H+h_o}\int_{0}^{2\pi}(\int_{0}^{R}I_2(\rho\le R)\rho d\rho+\int_{R}^{S}I_2(\rho>R)\rho d\rho)d\alpha\, dh} \quad (36)$$

Where Z_1' and Z_3' are as identified before in Table 3.

In the case of a co-axial cylindrical source with radius greater than the radius of the detector, there are two probabilities to be considered; the first probability that the lateral distance of the source is smaller than the detector circular face radius, i.e. ρ ≤ R and the second probability that the lateral distance of the source is greater than the detector circular face radius, i.e. ρ > R and in the two cases, there is only one path to the photon for the way out from the source which is exit from the base and is given by:

$$t_1=\frac{h-h_o}{\cos\theta} \quad (37)$$

Where h_o is the distance between the source active volume and the detector upper surface. The self attenuation factor of the source matrix S_{self} is as identified before in Eq. (18) and the average path length $\bar{t}$ travelled by a photon inside the source is given by:

$$\bar{t}=\bar{t}(t_1)=\frac{\int_{h_o}^{h_o+H}\int_{0}^{\pi}\int_{0}^{R}g_1\rho d\rho d\alpha dh+\int_{h_o}^{h_o+H}\int_{0}^{\pi}\int_{R}^{S}g_2\rho d\rho d\alpha dh}{\int_{h_o}^{h_o+H}\int_{0}^{\pi}\int_{0}^{R}I_2(\rho\le R)\rho d\rho d\alpha dh+\int_{h_o}^{h_o+H}\int_{0}^{\pi}\int_{R}^{S}I_2(\rho>R)\rho d\rho d\alpha dh} \quad (38)$$

where

$$g_1=\pi\int_{0}^{\theta_2}t_1\sin\theta\, d\theta+\int_{\theta_2}^{\theta_4}\varphi_{\max}t_1\sin\theta\, d\theta \quad (39)$$

$$\begin{aligned}g_2&=\int_{\theta_1}^{\theta_1'}\int_{0}^{\varphi'_{\max}}t_1\sin\theta d\varphi d\theta+\int_{\theta_1'}^{\theta_c}\int_{0}^{\varphi_c}t_1\sin\theta d\varphi d\theta+\int_{\theta_c}^{\theta_4}\int_{o}^{\varphi_{\max}}t_1\sin\theta d\varphi d\theta\\&=\int_{\theta_1}^{\theta_1'}\varphi'_{\max}t_1\sin\theta d\theta+\int_{\theta_1'}^{\theta_c}\varphi_c t_1\sin\theta d\theta+\int_{\theta_c}^{\theta_4}\varphi_{\max}t_1\sin\theta d\theta\end{aligned} \quad (40)$$

If t_B is the source container bottom thickness, so, there is only one path of the photon for the way out from the source container which is the exit from the base and is given by:

$$t_1'''=\frac{t_B}{\cos\theta} \quad (41)$$

The attenuation factor of the container material S_{sc} is as identified before in Eq. (27) and the average path length t_c travelled by a photon inside the source container is expressed as:

$$\overline{t_c}=\bar{t}(t_1''') \quad (42)$$

3. Experimental Setup

The full-energy peak efficiency values are carried out for two NaI (Tl) detectors with resolutions 8.5% and 7.5% at the 662 keV peaks of ^{137}Cs labeled as Det.1 and Det.2

respectively. The manufacturer parameters and the setup values are shown in Table 4.

The sources are polypropylene (PP) plastic vials of volumes 25 mL and 400 mL filled with an aqueous solution containing ^{152}Eu radionuclide which emits γ-ray in the energy range from 121 keV to 1408 keV, Table 5 shows sources dimensions. The efficiency measurements are carried out by positioning the sources over the end cap of the detector. In order to minimize the dead time, the activity of the sources is prepared to be (5048 ± 49.98 Bq). The measurements are carried out to obtain statistically significant main peaks in the spectra that are recorded and processed by winTMCA32 software made by ICx Technologies. Measured spectrum which saved as spectrum ORTEC files can be opened by ISO 9001 Genie 2000 data acquisition and analysis software made by Canberra. The acquisition time is high enough to get at least the number of counts 20,000, which make the statistical uncertainties less than 0.5%. The spectra are analyzed with the program using its automatic peak search and peak area calculations, along with changes in the peak fit using the interactive peak fit interface when necessary to reduce the residuals and error in the peak area values. The peak areas, the live time, the run time and the start time for each spectrum are entered in the spreadsheets that are used to perform the calculations necessary to generate the efficiency curves.

Table 4. The Manufacturer Parameters and the Setup Values

Items	Det.1	Det.2
Manufacturer	Canberra	Canberra
Serial Number	09L 654	09L 652
Detector Model	802	802
Type	Cylindrical	Cylindrical
Mounting	Vertical	Vertical
Resolution (FWHM) at 662 keV	8.5%	7.5%
Cathode to Anode voltage	+1100 V dc	+1100 V dc
Dynode to Dynode	+80 V dc	+80 V dc
Cathode to Dynode	+150 V dc	+150 V dc
Tube Base	Model 2007	Model 2007
Shaping Mode	Gaussian	Gaussian
Detector Type	NaI (Tl)	NaI (Tl)
Weight (kg)	0.77	1.8
Crystal Volume(cm3)	103	347.64
Crystal Diameter (mm)	50.8	76.2
Crystal Length (mm)	50.8	76.2
Top cover Thickness(mm)	Al (0.5)	Al (0.5)
Side cover Thickness(mm)	Al (0.5)	Al (0.5)
Reflector – Oxide (mm)	2.5	2.5
Outer Diameter(mm)	57.2	80.9
Outer Length(mm)	53.9	79.4

Table 5. Parameters of the Sources

Items	Source Volume (mL)	
	25	400
Outer diameter (mm)	32.1	113.89
Height (mm)	36.21	42.25
Wall thickness (mm)	1.2	2.03
Activity (Bq)	5048 ± 49.98	5048 ± 49.98

4. Results and Discussion

The full-energy peak efficiency values for all NaI (Tl) detectors are measured as a function of the photon energy using the following equation

$$\varepsilon(E) = \frac{N(E)}{T\ A_S\ P(E)} \prod C_i \qquad (43)$$

Where N(E) is the number of counts under the full-energy peak that is determined using Genie 2000 software, T is the measuring time (in second), P(E) is the photon emission probability at energy E, A_S is the radionuclide activity and C_i are the correction factors due to dead time and radionuclide decay. In these measurements of low activity sources, the dead time always less than 3%. So the corresponding factor is obtained simply using ADC live time. The statistical uncertainties of the net peak areas are smaller than 0.5% since the acquisition time is long enough to get the number counts at least 20,000 counts. The background subtraction is done. The decay correction C_d for the calibration source from the reference time to the run time is given by:

$$C_d = e^{\lambda \Delta T} \qquad (44)$$

Where λ is the decay constant and ΔT is the time interval over which the source decays corresponding to the run time. The main source of uncertainty in the efficiency calculations is the uncertainties of the activities of the standard source solutions. Once the efficiencies have been fixed by applying the correction factors, the overall efficiency curve is obtained by fitting the experimental points to a polynomial logarithmic function of the fifth order using a non linear least square fit[18]. In this way, the correlation between data points from the same calibrated source has been included to avoid the overestimation of the uncertainty in the measured efficiency. The uncertainty in the full-energy peak efficiency σ_ε is given by:

$$\sigma_\varepsilon = \varepsilon \sqrt{\left(\frac{\partial \varepsilon}{\partial A}\right)^2 \sigma_A{}^2 + \left(\frac{\partial \varepsilon}{\partial P}\right)^2 \sigma_P{}^2 + \left(\frac{\partial \varepsilon}{\partial N}\right)^2 \sigma_N{}^2} \qquad (45)$$

Where σ_A, σ_P and σ_N are the uncertainties associated with the quantities A_S, P(E) and N(E) respectively. Figs. 4 and 5 show the full-energy peak efficiencies for both NaI (Tl) detectors (Det.1 and Det.2) which include measured, calculated with S_{self} and calculated without S_{self} for cylindrical sources (25 mL and 400 mL) placed at the end cap of the detector as functions of the photon energy. Obviously, the non inclusion of the self attenuation factor in the calculations caused an increase in the full energy peak efficiency values. So to get correct results; the self attenuation factor must be taken into consideration. The percentage deviations between the calculated (with and without S_{self}) and the measured full-energy peak efficiency values are calculated by:

$$\Delta_1 \% = \frac{\varepsilon_{\text{cal-with } S_{self}} - \varepsilon_{meas}}{\varepsilon_{\text{cal-with } S_{self}}} \times 100 \qquad (46)$$

$$\Delta_2\,\% = \frac{\varepsilon_{\text{cal-without } S_{self}} - \varepsilon_{meas}}{\varepsilon_{\text{cal-without } S_{self}}} \times 100 \qquad (47)$$

where $\varepsilon_{\text{cal-with Sself}}$, $\varepsilon_{\text{cal-without Sself}}$ and ε_{meas} are the calculated with / without self attenuation factor and experimentally measured efficiencies, respectively. Table 6 shows the comparison between the percentage deviations Δ_1% and Δ_2% for different volumes placed at the end cap of NaI (Tl) detectors.

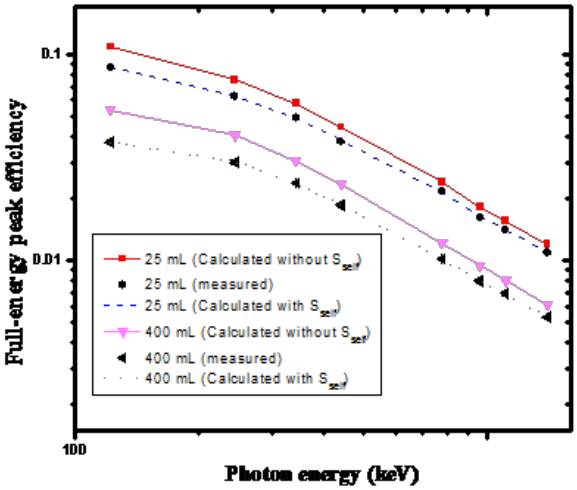

Figure 4. The full-energy peak efficiencies of a NaI(Tl) detector (Det.1); measured, calculated with S_{self} and calculated without S_{self} for different cylindrical sources placed at the end cap of the detector as functions of the photon energy

Table 6. The comparison between the percentage deviations Δ1% and Δ2% for different volumes placed at the end cap of different NaI (Tl) detectors

Detector	Energy (keV)	Source Volume (mL)			
		25		400	
		Δ_1%	Δ_2%	Δ_1%	Δ_2%
Det.1	121.78	0.11	20.30	-0.20	30.45
	244.69	0.25	16.91	0.71	26.10
	344.28	-0.48	14.47	-1.31	21.91
	443.97	1.33	14.80	0.10	21.19
	778.90	-1.05	9.87	-0.54	16.43
	964.13	1.51	11.19	0.51	15.82
	1112.11	0.44	9.60	-1.52	13.14
	1408.01	0.34	8.50	0.48	13.32
Det.2	121.78	0.03	20.31	-0.06	31.34
	244.69	0.14	16.87	-0.43	25.94
	344.28	0.01	14.93	0.02	23.57
	443.97	-0.63	13.14	-0.55	21.27
	778.90	0.10	10.93	-1.36	16.24
	964.13	0.80	10.58	-0.07	15.78
	1112.11	-0.39	8.88	-1.37	13.70
	1408.01	0.40	8.58	0.45	13.67

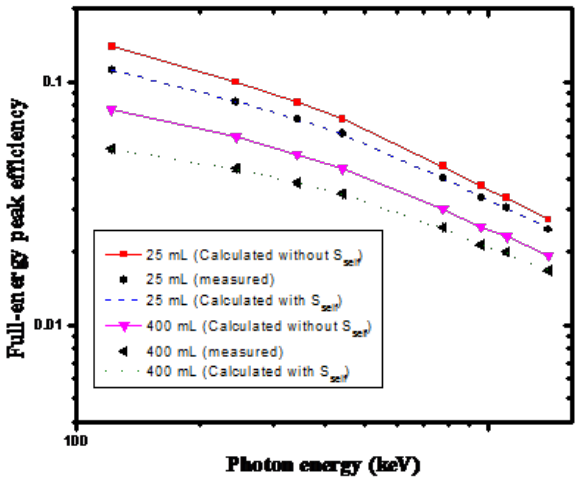

Figure 5. The full-energy peak efficiencies of a NaI(Tl) detector (Det.2); measured, calculated with S_{self} and calculated without S_{self} for different cylindrical sources placed at the end cap of the detector as functions of the photon energy

5. Conclusions

A direct analytical approach for calculating the full-energy peak efficiency has been derived. In addition, the self attenuation factor of source matrix, the attenuation factors of the source container and the detector housing materials have been calculated. The discrepancies between calculated with S_{self} and measured full-energy peak efficiency values were found to be less than (1.5%) while, between calculated without S_{self} and measured full-energy peak efficiency values were found to be less than (32%). The examination of the present results as given in tables and figures reflects the importance of considering the self attenuation factor in studying the efficiency of any detector using volumetric sources.

ACKNOWLEDGEMENTS

The authors would like to express their sincere thanks to Prof. Dr. Mahmoud. I. Abbas, Faculty of Science, Alexandria University, for the very valuable professional guidance in the area of radiation physics and for his fruitful scientific collaborations on this topic.

Dr. Mohamed. S. Badawi would like to introduce a special thanks to The Physikalisch-Technische Bundesanstalt (PTB) in Braunschweig, Berlin, Germany for fruitful help in preparing the homemade volumetric sources.

REFERENCES

[1] Perez, A. A., and Pibida, L., 2004, Performance of CdTe, HpGe and NaI(Tl) detectors for radioactivity measurements. Appl. Radiat. Isot. 60, 41-47.

[2] Vargas, M. J., Timón, A. F., Díaz, N. C., Sánchez, D. P., 2002, Monte Carlo simulation of the self-absorption corrections for natural samples in gamma-ray spectrometry. Appl. Radiat. Isot. 57, 893-898.

[3] Korun, M., 2002, Measurement of the average path length of gamma-rays in samples using scattered radiation. Appl. Radiat. Isot. 56, 77-83.

[4] Lippert, J., 1983, Detector-efficiency calculation based on point-source measurement. Appl. Radiat. Isot. 34, 1097-1103.

[5] Moens, L., and Hoste, J., 1983, Calculation of the peak efficiency of high-purity germanium detectors. Appl. Radiat. Isot. 34, 1085-1095.

[6] Haase, G., Tait, D., Wiechon, A., 1993, Application of new Monte Carl method for determination of summation and self-attenuation corrections in gamma spectrometry. Nucl. Instrum. Methods A336, 206-214.

[7] Sima, O., and Arnold, D., 1996, Self-attenuation and coincidence summing corrections calculated by Monte Carlo simulations for gamma-spectrometric measure- ments with well-type germanium detectors. Appl. Radiat. Isot. 47, 889-893.

[8] Wang, T. K., Mar, W.Y., Ying, T. H., Liao, C. H., Tseng, C. L., 1995, HPGe detector absolute-peak-efficiency calibration by using the ESOLAN program. Appl. Radiat. Isot. 46, 933-944.

[9] Wang, T. K., Mar, W. Y., Ying, T. H., Tseng, C. H., Liao, C. H., Wang, M.Y., 1997, HPGe Detector efficiency calibration for extended cylinder and Marinelli- beaker sources using the ESOLAN program. Appl. Radiat. Isot. 48, 83-95.

[10] Abbas, M. I., 2001, A direct mathematical method to calculate the efficiencies of a parallelepiped detector for an arbitrarily positioned point source. Radiat. Phys. Chem. 60, 3-9.

[11] Abbas, M. I., 2001, Analytical formulae for well-type NaI(Tl) and HPGe detectors efficiency computation. Appl. Radiat. Isot. 55, 245-252.

[12] Abbas, M. I., and Selim, Y. S., 2002, Calculation of relative full-energy peak efficiencies of well-type detectors. Nucl. Instrum. Methods A 480, 651-657.

[13] Selim, Y.S., Abbas, M. I., Fawzy, M. A., 1998, Analytical calculation of the efficiencies of gamma scintillators. Part I: total efficiency of coaxial disk sources. Radiat. Phys. Chem. 53, 589-592.

[14] Selim, Y.S., and Abbas, M. I., 2000, Analytical calculations of gamma scintillators efficiencies. Part II: total efficiency for wide coaxial disk sources. Radiat. Phys. Chem. 58, 15-19.

[15] Abbas, M. I., 2006, HPGe detector absolute full-energy peak efficiency calibration including coincidence correction for circular disc sources. J. Phys. D: Appl. Phys. 39, 3952-3958.

[16] Abbas, M. I., Nafee, S.S., Selim, Y.S., 2006, Calibration of cylindrical detectors using a simplified theoretical approach. Appl. Radiat. Isot. 64, 1057-1064.

[17] Nafee, S. S., and Abbas, M. I., 2008, Calibration of closed-end HPGe detectors using bar (parallelepiped) sources. Nucl. Instrum. Methods A 592, 80-87.

[18] Badawi, M. S., 2010, Ph.D. Dissertation. Alexandria University, Egypt.